JOURNAL OF PROPULSION AND POWER
Vol. 23, No. 5, September–October 2007

Physical Characterization of Aerosol Emissions from a Commercial Gas Turbine Engine

Prem Lobo,* Donald E. Hagen,† Philip D. Whitefield,‡ and Darryl J. Alofs§
University of Missouri–Rolla, Rolla, Missouri 65409

DOI: 10.2514/1.26772

This paper discusses the results of the Aircraft Particle Emissions Experiment Project for the physical characterization of total (nonvolatile plus volatile) aerosol emissions (emission factors, hydration properties, and distribution shape parameters) by extractive sampling from an on-wing CFM56-2C1 engine. Samples were extracted at the engine exit plane (1 m) as well as locations 10 and 30 m downstream. Three different fuels were used in this study: base fuel, high-sulfur fuel, and high-aromatic fuel. For the 1 and 10-m probe locations, strong and sometimes nonlinear dependencies were observed on fuel flow rate and no statistically significant dependencies were observed for fuel composition. At 30 m, the onset of gas-to-particle conversion was apparent for low- to medium-fuel flow rates. The soluble mass fraction was found to increase with distance from the engine exit plane and with increasing fuel aromatic and sulfur content. An intercomparison of gas and particle sampling trains showed that gas-to-particle conversion is a serious sample train artifact for gas sampling trains in which dilution cannot be achieved at the probe tip.

Nomenclature

EIn = number-based emission index
EIm = mass-based emission index

I. Introduction

JET engines are a significant source of soot particles in the atmosphere which, in contrast to most other combustion sources, are injected not only into the planetary boundary layer, but also into the upper troposphere and lower stratosphere [1–3]. Here their atmospheric residence time and hence, their potential environmental impact, are enhanced. Soot particles contribute to climate forcing both directly by strongly absorbing solar radiation, and indirectly through water-uptake and cloud activation [4–16]. They can interact with gaseous chemical species, especially in the near-field plume, and play a significant role in atmospheric chemistry [17,18]. Some modeling results indicate that the current commercial fleet of aircraft could be a noticeable source of soot near the tropopause at northern midlatitudes [19,20]. An additional concern, primarily in the vicinity of airports, is the contribution of aircraft emissions to the formation of photochemical smog and the delivery (through inhalation) of highly concentrated irritants into human beings [21,22]. As a consequence of the complex role of aviation-induced particles in the atmosphere, the physical and chemical characteristics of the particles emitted by gas turbine engines have been the focus of recent research programs, e.g., the NASA EXCAVATE (Experiment to Characterize Aircraft Volatile Aerosol and Trace-Species Emissions) program [23], and the European PartEmis (measurement and prediction of emissions of aerosols and gaseous precursors from gas turbine engines) project [24]. Among the key measurement parameters are size-resolved particle number distribution, total number density, and particle morphology, which are converted into size-resolved particle surface area and mass densities and concentrations as well as emission indices. These size distribution dependent characteristics control the particulate matter (PM) emissions' evolution in the atmosphere and their ability to influence the preceding processes. Project APEX (Aircraft Particle Emissions Experiment) is a recent collaborative research effort aimed at further addressing some of these issues.

The University of Missouri–Rolla (UMR) Center of Excellence for Aerospace Particulate Emissions Reduction Research was a team member for Project APEX performed at the NASA Dryden Flight Research Center (DFRC) at Edwards Air Force Base, California, in April 2004. This paper summarizes and describes the results of Project APEX from the UMR perspective, in terms of the physical characterization of total (nonvolatile plus volatile) aerosol emissions by extractive sampling from a NASA DC-8 aircraft with CFM56-2C1 engines. Samples were extracted at the engine exit plane (1 m) as well as locations 10 and 30 m downstream. Three different fuels were used in this study: a baseline JP-8 fuel (base fuel), base fuel doped with tertiary butyl disulfide (high-sulfur fuel), and Jet A fuel which had a considerably higher aromatic content than the two other fuels used (high-aromatic fuel). The base fuel consisted of 383 parts per million by mass (ppmm) sulfur and 17.6% aromatics, the high-sulfur fuel consisted of 1595 ppmm sulfur and 17.3% aromatics, and the high-aromatic fuel consisted of 530 ppmm sulfur and 21.6% aromatics. Fuel sulfur and aromatic concentrations reported are in parts per million mass and percent by volume, respectively. The aerosol measurements were designed to measure the emissions in the plume at the probe tip location. However, the extractive sampling process may result in sample modification due to inertial, thermophoretic, and diffusional effects. Corrections to account for some of these processes are discussed, but further studies are needed, especially to address effects at the probe tip. Finally, a discussion of measurements comparing gas vs particulate sampling trains is also included. The data presented are a summary of the first detailed study of the physical characterization of the PM emissions from a current in-service commercial class gas turbine engine (CFM56-2C1) as a function of engine operating condition and fuel composition, and as such, provides an introduction to the extensive NASA database from which it is derived. The data summarized here can be applied to

Received 25 July 2006; revision received 30 April 2007; accepted for publication 1 May 2007.

*Assistant Director, Center of Excellence for Aerospace Particulate Emissions Reduction Research, G-7 Norwood Hall; plobo@umr.edu. Member AIAA.

†Professor of Physics, and Director of Cloud and Aerosol Sciences Laboratory, Center of Excellence for Aerospace Particulate Emissions Reduction Research, G-7 Norwood Hall; hagen@umr.edu.

‡Professor and Chair of Chemistry, and Director of Center of Excellence for Aerospace Particulate Emissions Reduction Research, G-7 Norwood Hall; pwhite@umr.edu. Member AIAA.

§Professor of Mechanical Engineering, Center of Excellence for Aerospace Particulate Emissions Reduction Research, G-7 Norwood Hall; dalofs@umr.edu.

emissions estimation, plume evolution model development, and local air quality modeling applications.

II. Instrumentation

The instrumentation onboard the UMR mobile laboratory consisted of the Cambustion DMS500,[¶] a state-of-the-art fast particulate spectrometer, to gather real-time size distribution information and total concentration of engine exhaust particulates; a differential mobility analyzer (DMA) (TSI model 3071), a traditional and slower instrument to measure aerosol size distributions; a TSI condensation particle counter (CPC) (TSI model 3022) to measure total number concentration; a fast response carbon dioxide (CO_2) detector to monitor sample dilution and establish emission factors; a deliquescence system to measure total soluble mass fraction; a hygrometer to measure the sample's water content; and a weather station to monitor the ambient conditions of temperature, relative humidity, pressure, and wind speed and direction. These were employed in a standard configuration [25] which had been used on previous jet engine emissions sampling campaigns [26–33]. Traditional aerosol sizing techniques are either slow or have insufficient resolution to provide the database needed by modelers. Increased measurement speed is required because engine on-time for sampling is expensive, and some engine conditions, e.g., takeoff power, can be made available only for short times. Fast response instruments are required to make observations of engine transients between stable operating conditions. Project APEX was the first application of a new fast mobility spectrometer to gas turbine emissions characterization.

III. Application of a Novel Fast Aerosol Spectrometer

Project APEX afforded the first opportunity to apply a novel fast aerosol sizing instrument, the DMS500, to the PM emissions from a gas turbine engine. The DMS500 relies upon electrical mobility for particle sizing [34]. In this instrument, the aerosol sample is passed through a cyclone separator to remove particles larger than 1 μm and electrically charged with a corona charger. The electrically charged particle sample is then introduced into a strong electrical field established in a classifying column. The field forces the charged particles to drift toward an array of electrometers through a sheathing gas flow created in the column. The location at which a charged particle reaches the electrometer array depends on its aerodynamic drag/charge ratio. Real-time monitoring of the electrometer outputs provided a measure of the particle size distribution. The primary innovation of the DMS500, a fast size distribution measurement rate (up to 10 Hz), greatly enhanced the statistical reliability of size parameter measurement and afforded the opportunity to observe transient behavior in the engine emissions. The time needed for a size distribution measurement is dictated by the smear time associated with the transport of particles from probe to instrumentation, and by the need to collect a statistically meaningful sample. The aerosol which enters the sampling train at one point in time, exits it over a range of time (smear time) which can be estimated for both turbulent and laminar flow conditions. When a step change is made to the aerosol at the input end of the sample train, the smear time is the time required for the change detected at the output end to go from 10% of its new value to 90%. At Project APEX, the time required to measure a size distribution was typically 7 s, and was driven by the smear time.

The operating principle of the DMS500 is similar to the engine exhaust particle sizer (EEPS) spectrometer (TSI model 3090). In a recent study, the EEPS and traditional aerosol instrumentation like the scanning mobility particle sizing (SMPS) system and CPC were shown to compare favorably [35]. The DMS500, shown to compare well with SMPS systems in laboratory situations [36], also demonstrated excellent agreement with traditional aerosol instrumentation under field test conditions [37]. During Project APEX, the DMS500 was compared with a standard SMPS system for sizing and with a CPC for total concentration for the exhaust aerosol. They agreed to within 2% for number-based geometric mean diameter, 7% for mass-based geometric mean diameter, and 14% for total concentration. As a consequence of the good agreement between the DMS500 and conventional instrumentation for aerosol physical characterization, all the data and analysis presented in this paper are based upon the data set from the DMS500 unless otherwise specified.

[¶]http://www.cambustion.co.uk/instruments/dms500/

IV. Sampling Train and Line Loss

Probe rakes were located at three distances (1, 10, and 30 m) behind the engine exit plane to capture exhaust samples. A sampling train was used to transport these samples from the probes to the instrumentation. For the 1 m rake, the sample was diluted with a concentric flow of dry nitrogen 1.4 cm downstream from the probe tip, was carried through 1 m of 5.33 mm i.d. followed by 1.5 m of 4.83 mm i.d., and 1.8 m of 8.37 mm i.d. stainless steel tubing to a valve switching box, followed by 23.8 m of 15.75 mm i.d. stainless steel tubing to the NASA Langley Research Center (LaRC) distribution manifold. From here, the sample was distributed to the various research groups participating in the project. The sample was transported from the LaRC distribution manifold to the UMR DMS500 by 8 m of 7.9 mm i.d and 1.2 m of 10.7 mm i.d. stainless steel tubing. The purpose of the dilution was to inhibit water condensation, deposition of volatile material on soot particles or the creation of new volatile particles, inhibit particle coagulation, and bring particle concentrations down into the operating ranges of the instrumentation. The 10 m sample train was also diluted and was similar to that for the 1 m except that the long run of 15.75 mm i.d. tubing was of length 20.7 m. A large flow rate (1152 lpm) of exhaust gas at the 30 m location was drawn into a 29-m-long 48 mm i.d. stainless steel tube by a downstream blower. A cyclone was used to remove particles larger than 2.5 μm in diameter. The actual 30 m sample was drawn from this flow through a 7.4 mm i.d. stainless steel tube and transported 3 m to the LaRC distribution manifold. No additional dilution was provided here. Safety requirements dictated the long sample trains described herein, because the diagnostic instrumentation was required to be located beyond the wingtip of the wing which held the test engine. Further sampling train details, including a diagram, can be found in the NASA report [38].

Modification of the aerosol size spectrum due to line loss is an artifact associated with extractive sampling which must be accounted for with calibration experiments. Inertial, thermophoretic, and diffusional effects contribute to the loss of particles in the sampling train. The penetration of particles through a sampling system is size dependent. Thermophoretic losses at the probe tip are reported to be negligible [25] and those downstream of the probe, estimated based on a semi-empirical model [39], are found to be ~8%. In this study, thermophoretic losses were not evaluated; however, inertial and diffusional losses have been quantified by calibration and accounted for in the data presented, based on the assumption that the size distribution observed at the instruments applies to the entire sample train. This assumption will introduce additional uncertainty should gas-to-particle conversion occur throughout the sample line. Thus within these limits, the particle size distributions reported in this paper represent the nascent distributions in the exhaust stream at the point sampled.

The source aerosol used in line calibration studies must be stable and free of any volatile compounds and moisture as these have a tendency to induce nucleation and interact with soot particles, hence altering the size distribution within the sample lines. It is preferable for it to be a combustion source because the sampling train is used to transport combustion aerosols. The source aerosol must also have a sufficient population in the size regime of interest for gas turbine emissions (~8–200 nm). The sampling system design should minimize line length and aerosol transit time. Bends, flow meters, and valves in the sampling train should be avoided where possible, as these typically involve substantial loss.

A separate study to establish the penetration function of particles in the sampling train was conducted at NASA DFRC by UMR and

ARI (Aerodyne Research, Inc.). This experiment used a monodispersed sodium chloride (NaCl) aerosol as the calibration source. It was generated by atomizing an NaCl solution and then selecting a certain size aerosol using a DMA. CPCs were used to measure the concentration of the monodispersed aerosol at three locations for the 1 m sampling train: the probe tip and the ends of the sampling train to UMR and to ARI. The ratio of the concentration of aerosol at the end of either sampling train to the concentration at the probe tip provided the penetration factor (Pen) for the selected aerosol size. This experiment was repeated a number of times for different aerosol sizes (20–300 nm). The results of this experiment are shown in Fig. 1. The uncertainty in the measurement is represented by error bars which were calculated using one standard deviation in the averaged data set.

Although this experiment provided a crude estimate of the penetration function, it was decided that a thorough analysis be performed after the field test at UMR. The entire APEX probe assembly and sampling train was set up at UMR and the line loss experiment was repeated. For this more detailed penetration study, a combustion source and NaCl aerosols were used for the calibration experiment. The combustion source used in this study was exhaust generated from a diesel truck: a surrogate for a gas turbine engine. Lack of availability of a gas turbine engine and the costs associated with running such an engine made it impractical to use in this calibration experiment. Diesel emissions are well studied [40] and provide a reliable calibration source for line loss studies. In these studies, the diesel emissions were dried and diluted to remove unwanted volatile components. Several line loss calibrations were performed. The first was for the section of the sample train from probe tip to the LaRC distribution manifold. This segment was common to all aerosol samplers. The remainders were from the LaRC distribution manifold to each of the UMR aerosol monitoring instruments. The total penetration function for a given instrument is the product of the penetration functions for the common segment and that between the distribution manifold and the instrument.

The DMS500 was used to obtain the penetration as a function of size. It provided distinct advantages for such calibration measurements. With the DMS500, a poly-dispersed source could be employed to provide fast simultaneous size-dependent losses for particle diameters ranging from 5 to 1000 nm. As a consistency check, the line loss experiments were also repeated at selected sizes using a monodisperse NaCl aerosol and CPCs as was done at NASA DFRC. Figure 2a illustrates the comparison of the penetration as a function of size using the two different sources for the common segment from the inlet of the probe tip to the LaRC distribution manifold. The results of both posttest experiments and those performed at NASA DFRC are in reasonable agreement with each other. The fitted penetration function for the common sampling train segment based on all calibration data is presented in Fig. 2b. This function was provided to all aerosol experimenters for use in correcting their data for the common line loss. The large penetration losses at small particle diameters are an unavoidable consequence of diffusional transport loss [41,42], and it should be noted that for particle sizes less than 20 nm, substantial penetration corrections have been made. All the data presented in this paper have been corrected for line losses from the probe tip to the instruments.

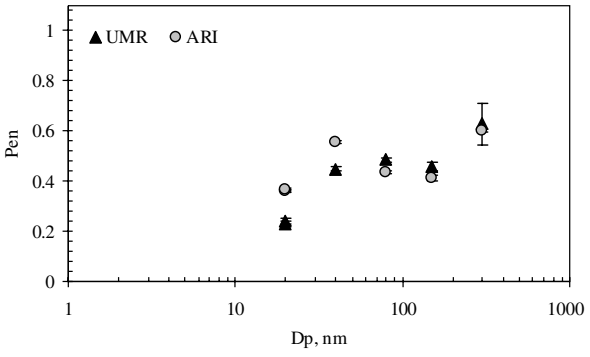

Fig. 1 Results of the line loss calibration experiment performed at NASA DFRC for the UMR and ARI sample trains.

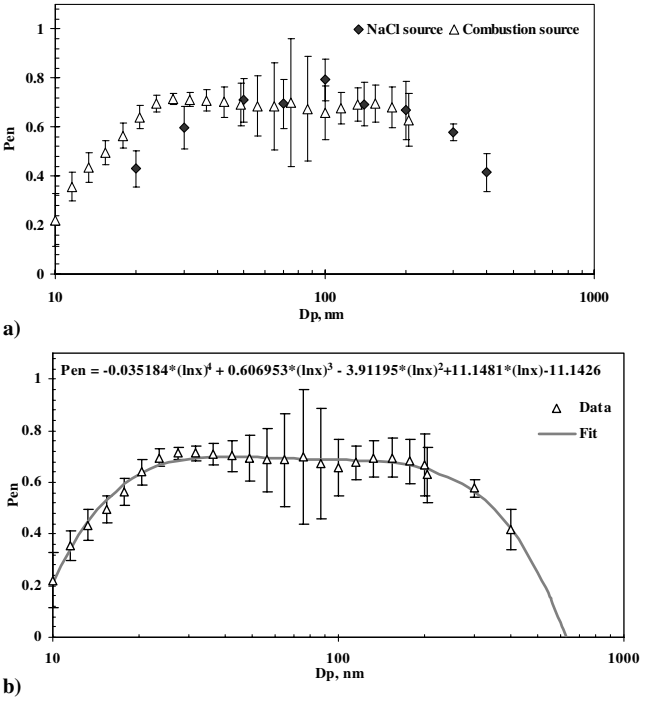

Fig. 2 Penetrations as a function of size from probe tip to LaRC distribution manifold: a) comparison of NaCl and combustion sources and b) final-fitted APEX penetration function.

V. Results and Discussion of the APEX Data Set

A. Size Distributions

Gas turbine engine emissions are influenced by engine power settings and ambient conditions at the engine inlet. The formation of soot and its partial oxidation in gas turbine combustors are very complex processes that are still being studied [3,43,44]. Changes in the combustor environment (higher temperatures and pressures, different injector systems, etc.) contribute to the variation in particle size distributions measured downstream at the engine exit plane. Figures 3a and 3b show typical particle size distributions as a function of engine power taken at the 1 and 30 m probe locations, respectively, when the engine was burning the base fuel.

For discussions of the influence of test operating conditions, e.g., fuel type, fuel flow rate, etc., on the exhaust aerosol, it is convenient to represent the size distributions with characteristic parameters: number-based geometric mean diameter (Dgeom), geometric standard deviation (Sigma), mass-based geometric mean diameter (DgeomM), and total concentration; and the derived size-dependent parameters: number-based emission index EIn and mass-based emission index EIm. The number-based geometric mean diameter gives a measure of (the exponential of) the average particle logarithmic diameter for the particulate size distribution, i.e., an average value in log diameter space and the geometric standard deviation gives a measure of its width. The geometric rather than arithmetic mean is used because size distributions are customarily plotted on a logarithmic scale. The mass weighted geometric diameter gives the corresponding mean diameter for the mass distribution vs size. Because of the diameter cubed dependence of particle mass, the mass-based geometric mean gives more emphasis to the large particle portion of the size distribution compared with the number-based geometric mean. The number-based emission index is the number of particles per kilogram fuel burned and can be calculated by

$$\mathrm{EI}\,n = \mathrm{EI}_{\mathrm{CO_2}} \frac{N_0}{M(\mathrm{CO_2})} \tag{1}$$

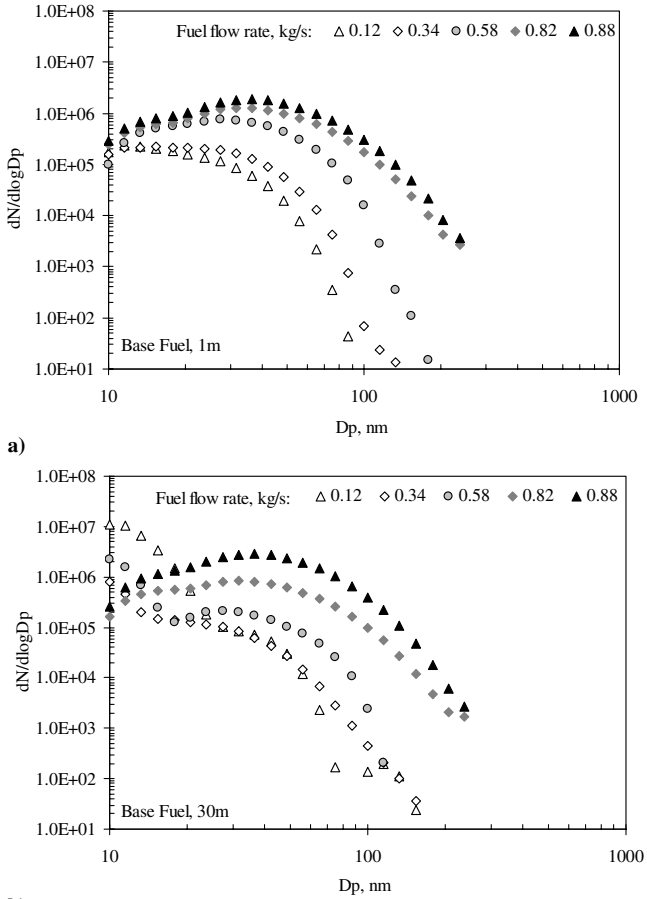

Fig. 3 Variation of particle size distributions with changes in fuel flow rate for the base fuel: a) 1 m and b) 30 m.

where EI_{CO_2} denotes the mass emission index of CO_2 (for aircraft engines $EI_{CO_2} = 3160$ g/kg, and $M(CO_2)$ denotes the mass of CO_2 per volume exhaust sample, which is calculated by multiplying measured CO_2 mixing ratios with $(44/29)\rho_{air}$, where ρ_{air} is the air density and 44/29 is the molar mass ratio of CO_2 and air. The mass-based emission index is the mass of particles per kilogram fuel burned and its calculation is analogous to that for EIn, and is given by

$$EI\,m = EI_{CO_2}\frac{M(N_0)}{M(CO_2)} \tag{2}$$

where $M(N_0)$ is the mass of aerosol per unit volume of exhaust sample.

By way of example, Table 1 presents the average values for these parameters at two different fuel flow rates for the base fuel at the 1 m sampling location. It should be noted, however, that although these parameters provide a useful summary of the size-dependent data, they do not contain all of the information available in the original distributions.

Table 1 Total aerosol parameters for two fuel flow rates (base fuel, 1 m)

Parameter	0.12 kg/s	0.87 kg/s
Dgeom, nm	18.53 ± 1.35	33.27 ± 0.69
Sigma	1.49 ± 0.09	1.80 ± 0.02
DgeomM, nm	34.87 ± 11.85	84.74 ± 1.13
EIn, 10^{15}/kg fuel	0.43 ± 0.16	1.99 ± 0.48
EIm, g/kg fuel	0.004 ± 0.002	0.17 ± 0.04

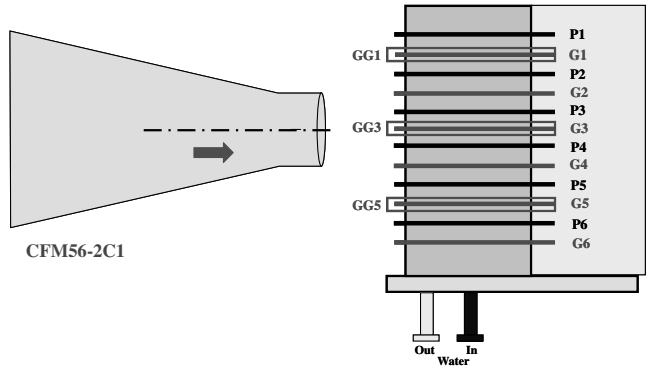

Fig. 4 Orientation of sampling probes (P-particulate, G-gaseous, GG-external gaseous) with respect to the engine exit plane.

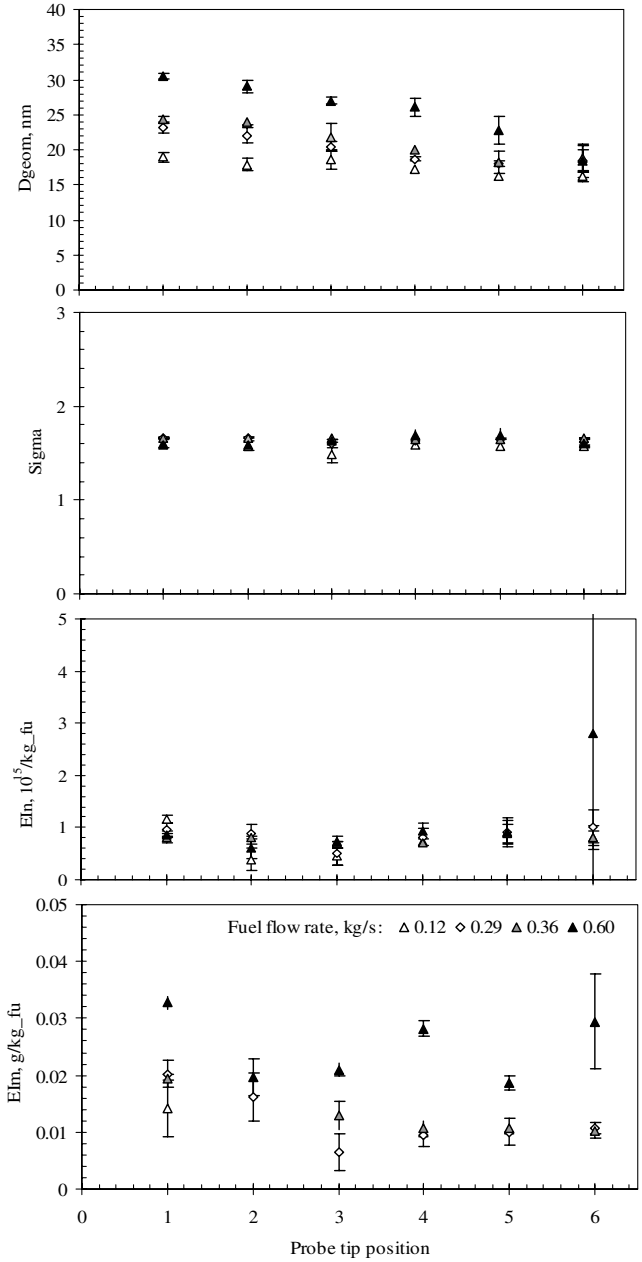

Fig. 5 Variation in aerosol parameters for different probe tip positions on the 1m rake as a function of fuel flow rate.

B. Mapping Sequence

A mapping sequence was performed to study the spatial variation of the emissions across the engine's exit plane, and to determine the optimal probe tip position from which to sample. This study was limited to the fixed locations and dimensions of the 1 m sampling rake. The orientation of the various sampling probes with respect to the engine exit plane is presented in Fig. 4.

Figure 5 details the variation in the aerosol parameters (geometric mean diameter, geometric standard deviation, number and mass-based emission indices) for the different probe tip positions on the 1 m rake as a function of fuel flow rate. Some spatial variation of aerosol parameters was observed. The PM samples obtained from probe tip position 3 were determined to be representative of the core exhaust flow. Measurements from an adjacent gaseous probe revealed that emission indices for NO_x, CO, and HC agreed well with the engine manufacturer's predictive models [38] and with the values from the International Civil Aviation Organization databank [45] for this class of engine. Thus, probe tip position 3 best represented the overall spatial averages for all aerosol parameters calculated and was subsequently used as the main probe tip for sampling particles.

C. Sampling Sequences

There were two types of sampling sequences; one focusing on the landing–takeoff cycle [U.S. Environmental Protection Agency (EPA) sequence] and the other targeting a parametric study (NASA sequence) [38]. There were three EPA sampling sequences with the following matrix of power conditions and sampling durations: 7% (17 min), 100% (0.7 min), 85% (2.2 min), 30% (4 min), 7% (17 mins). The first two EPA sequences were performed using the base fuel and the third used high-sulfur fuel.

There were a total of six NASA sampling sequences that included the following power conditions and sample duration times: 4% (4 min), 100% (1.5 min), 85% (4 min), 70% (4 min), 65% (4 min), 40% (4 min), 30% (4 min), 15% (4 min), 7% (4 min), 4% (4 min). Sequences 1 and 2 used the base fuel, sequences 3 and 4 used high-sulfur fuel, and sequences 5 and 6 used high-aromatic fuel.

Table 2 Comparison of slope and R^2 values for the 1 and 10 m probe data

Probe location	Fuel	Slope	R^2
1 m	base	19.9 ± 0.3	0.82
	high aromatic	21.5 ± 0.3	0.96
	high sulfur	21.6 ± 0.4	0.98
10 m	base	24.7 ± 0.2	0.96
	high aromatic	25.0 ± 0.3	0.95
	high sulfur	23.4 ± 0.2	0.99

Figures 6–8 represent the variation in parameters measured as a function of fuel flow rate for the three different fuels. The entire set of runs encompassing both the NASA and EPA sequences are represented in these plots.

1. *Geometric Mean Diameter (Fig. 6)*

Dgeom generally increases with increasing fuel flow rate for all three fuels and all three probe locations and ranges from 12–35 nm. For the 1 and 10 m data, Dgeom is linear with respect to fuel flow rate. The slope and R^2 values from a linear fit to the data and are presented in Table 2. Similar slopes are observed at both sampling locations, and in all cases the R^2 values are near unity.

For the data from the 30 m probe location, the linear relationship is not observed. At low-fuel flow rate, ≤ 0.6 kg/s, Dgeom is small ($\sim$12 nm) and relatively constant. It increases significantly at fuel flow rates >0.6 kg/s, rising to $\sim$18 nm at 0.8 kg/s for most measurements and to 27 nm in some cases. These observations are compatible with the onset of gas-to-particle conversion in the near-field plume, i.e., an initial soot distribution is modified through condensation of volatile compounds (H_2SO_4 and volatile hydrocarbons) resulting in the creation of both new particles and growth of existing soot particles. Evidence for this can be seen in Fig. 3, with the clear appearance of new small particle modes in the 30 m data compared with 1 m. The extent of these processes will

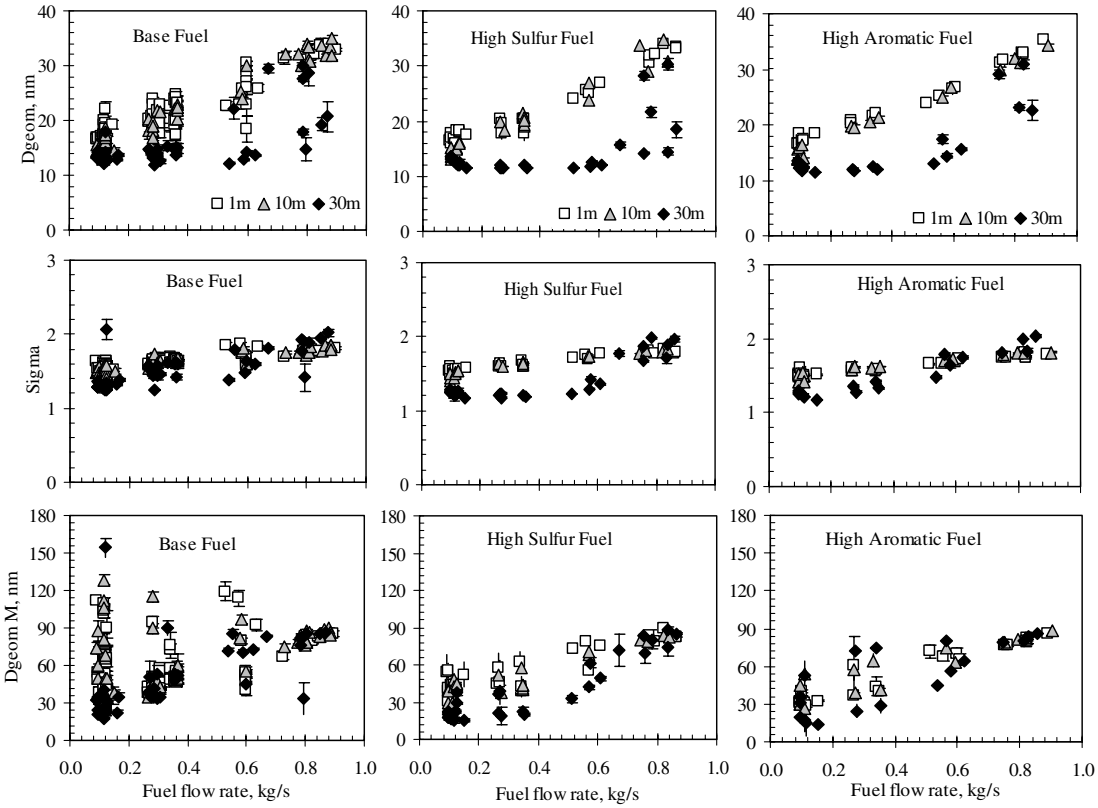

Fig. 6 Variation in Dgeom, Sigma, and DgeomM with fuel flow rate for the entire set of runs (NASA and EPA sequences) performed using three different fuels.

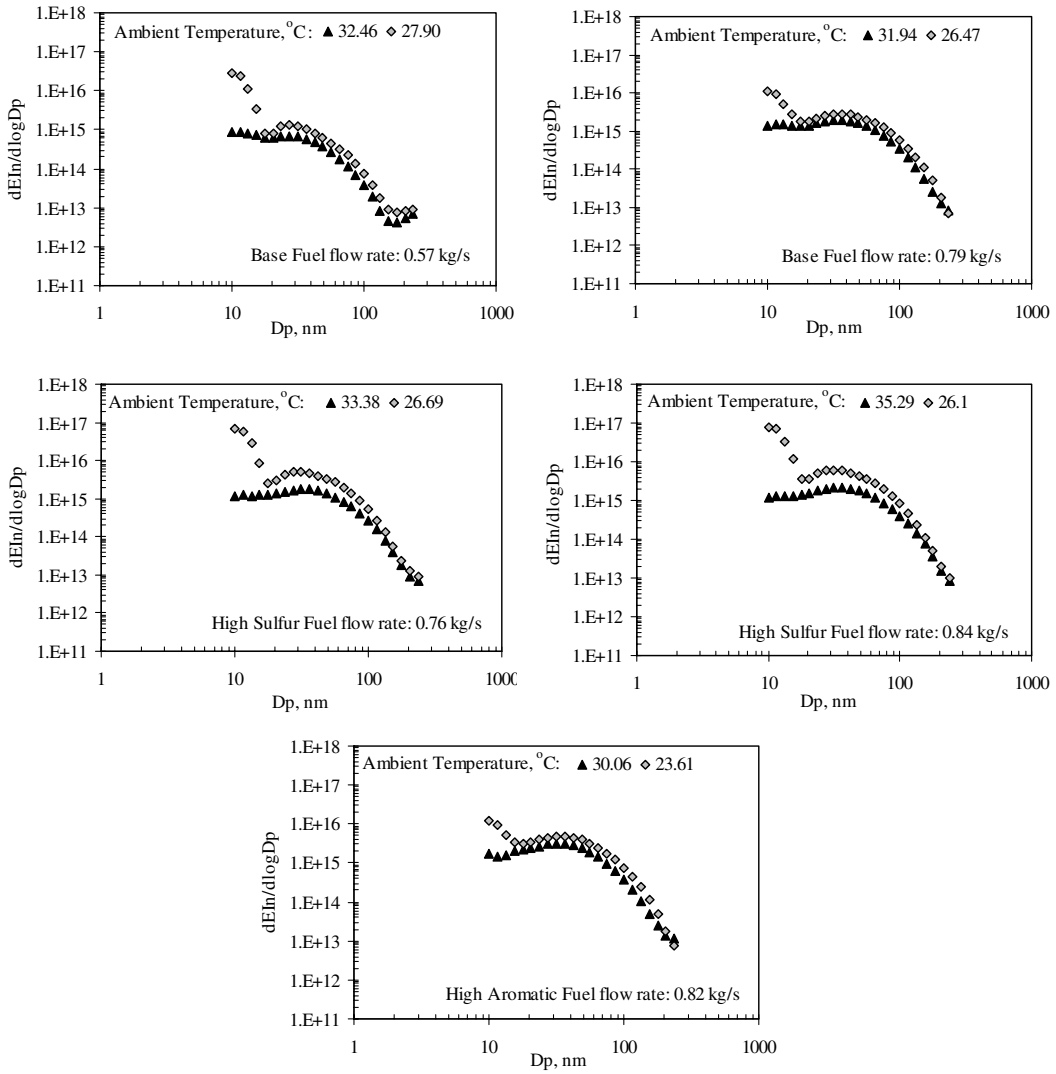

Fig. 7 Variation in particle size distributions of two independent runs at 30 m probe location performed at different ambient temperatures with three fuels at medium- to high-fuel flow rates.

depend on the temperature, dilution, and flow characteristics of both the exhaust plume and the flow through the sampling lines. Based on model predictions [46], volatile components detected in the 30 m downstream probe were most likely formed by gas-to-particle conversion in the sample lines. This process may mimic that occurring naturally in the near-field plume under appropriate atmospheric conditions, but until these effects can be adequately modeled it will not be possible to deconvolute the 30 m data to yield information on the natural evolution of the aerosol in the exhaust plume. It is important to note that significant gas-to-particle conversion is not present in the 1 and 10 m data suggesting that such processing is mitigated through careful probe tip dilution.

Low-fuel flow rates correspond to relatively low linear velocities in the exhaust flow and longer residence times before the flow reaches the 30 m probe. Hence at low-fuel flow rates, more time is available for nucleation processes to boost the aerosol population at the small size end of the spectrum, canceling out the increase in mean size with increasing fuel flow rate observed at 1 and 10 m. At high-fuel flow rates, the residence time in the plume is less and the exhaust gas temperature is higher, both conditions tend to suppress nucleation. The data for fuel flow rates >0.15 kg/s is similar for the 1 and 10 m locations, suggesting that the gas-to-particle processes become significant in the near-field plume, becoming more pronounced as plume residence time increases. At higher fuel flow rates, two sets of Dgeom are observed in the 30 m data. This observation is also compatible with nucleation being active in the near-field plume. For the runs exhibiting the larger Dgeom, the ambient temperature was significantly higher (see Fig. 9). This higher temperature air, when entrained into the plume, would suppress nucleation, lowering the population of the nucleation small particle mode, and thereby increasing Dgeom.

2. Geometric Standard Deviation (Fig. 6)

The geometric standard deviation is related to the width of the size distribution: Half width = Dgeom (Sigma − 1). Sigma shows fuel flow dependencies similar to those for Dgeom. At 1 and 10 m, it tends to increase with increasing fuel flow rate and is independent of fuel type. At 30 m, it tends to be constant at low-fuel flow rate but increases significantly at high-fuel flow rate. Nucleation arguments similar to those just given for Dgeom can be made for Sigma. When the nucleation increases the population of small particles, while keeping the large particle population constant, the size distribution widens. Sigma generally varies from 1.2–2.0. This increase in Sigma represents a half-width variation from 2.8–34 nm.

3. Mass-Based Geometric Mean Diameter (Fig. 6)

DgeomM generally increases with increasing fuel flow rate for all three probe locations and all three fuels. This is consistent with the Dgeom behavior. Also there is more scatter in the data in the low-to medium-fuel flow rate regime, whereas there is little scatter at high-fuel flow rate, an effect not observed in Dgeom. This can be attributed to the onset of nucleation in the near-field plume. At low-to medium-fuel flow rate, Dgeom and Sigma are small. The small size end of the

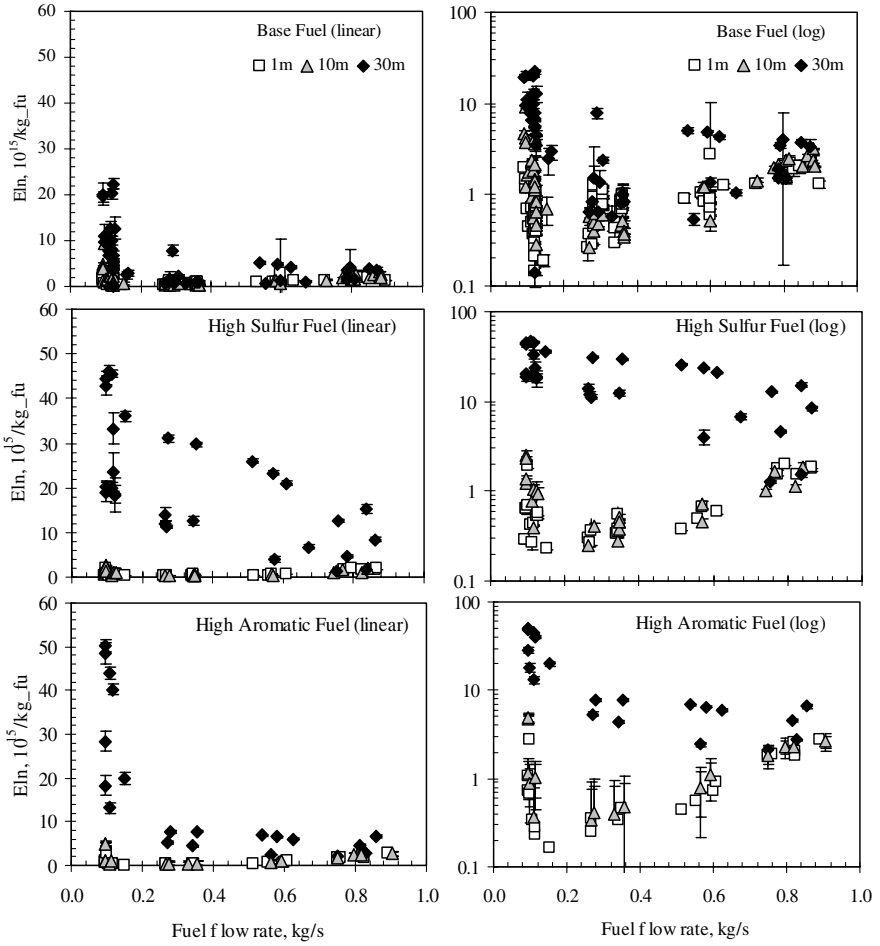

Fig. 8 Variation in EI*n* with fuel flow rate for entire set of runs performed (NASA and EPA sequences) using three different fuels.

size spectrum is the region where nucleation and fluctuations in nucleation have their largest impact on its DgeomM. At high-fuel flow rate, Dgeom and Sigma are relatively large. Because DgeomM is more heavily weighted toward the large size end of the size spectrum, nucleation has a lower impact. In this size range, it produces few large particles, and those that it does produce have a reduced impact on DgeomM because of the relatively large Sigma at high-fuel flow rate.

4. Number-Based Emission Index (Fig. 8)

For all three fuels, at the 1 and 10 m locations, EI*n* is higher at the lower fuel flow rates (0.1 kg/s) and highest fuel flow rates (0.85 kg/s) with a minimum occurring between 0.2–0.4 kg/s. The variation in EI*n* at 1 and 10 m for different fuel flow rates is not statistically significant. There is, however, a difference in EI*n* between the 1 and 30 m probe locations. At the 30 m probe location, EI*n* is highest at the lowest fuel flow rates, and is an order of magnitude higher than that for the 1 and 10 m cases. It then decreases with increasing fuel flow rate until ∼0.75 kg/s is reached, where it becomes constant. The greatest differences between the 1 and 30 m data are observed at low-fuel flow rates where the residence time in the plume affords more opportunity for gas-to-particle conversion to occur resulting in larger EI*n* values. The increase in EI*n* at 30 m compared to 1 m is most pronounced for the high-sulfur fuel. This is also observed for the high-aromatic fuel, though the effect is less pronounced.

5. Mass-Based Emission Index (Fig. 9)

For all three fuels, at all three probe locations, EI*m* tends to increase with fuel flow rate, with a low-fuel flow rate minimum between 0.1 and 0.25 kg/s, and a high-fuel flow rate maximum between 0.75 and 0.9 kg/s. The variation in EI*m* at 1 and 10 m for different fuel flow rates is not statistically significant. At high-fuel flow rates, the EI*m* values for the 1 and 30 m cases converge suggesting that the mass at these higher fuel flow rates is dominated by the nonvolatile component of the aerosol. See DgeomM behavior discussed in Sec. V.C.3.

D. Deliquescence

The evolution of combustion particles in the atmosphere is strongly influenced by their ability to interact with water vapor. This characteristic was investigated with a deliquescence technique [47–49], where a tandem DMA with an intermediate saturator was used to measure the particles' dry and wet diameters. From this information, the particles' critical supersaturation or soluble mass fraction (SMF) was determined. In this study, two classes of particles were measured. These had dry diameters of approximately 40 and 60 nm. The deliquescence results for both classes of particle diameters over all fuel flow rates and plume sampling locations are combined in Fig. 10.

The SMF increases with distance from the engine exit plane. This is reasonable, as the longer the residence time in the plume, the greater is the opportunity for gas-to-particle conversion. Increasing fuel aromatic and sulfur content were observed to increase the SMF. At the engine exit plane (∼1 m), the particles contain essentially no soluble material because it was too hot for condensation processes to occur. Furthermore, the sample was diluted before it was allowed to cool in the sampling train, thus preventing any condensation downstream during sample transport. There was no statistical difference in SMF between the 1 and 10 m probe locations, which is consistent with the absence of gas-to-particle conversion in the 1–10 m regime of the plume. Evidence of gas-to-particle conversion was observed at the 30 m probe. Here the average SMF values and their standard deviations are 0.057 ± 0.026 for the base fuel,

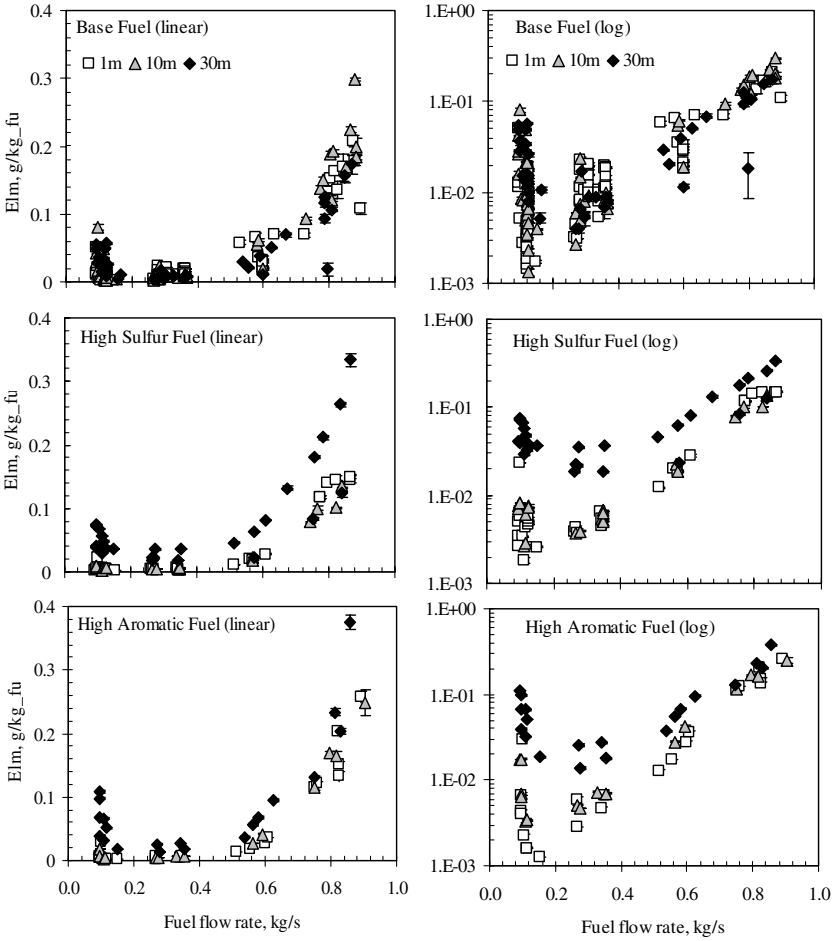

Fig. 9 Variation in EI*m* with fuel flow rate for the entire set of runs performed (NASA and EPA sequences) using three different fuels.

0.115 ± 0.076 for the high-aromatic fuel, and 0.151 ± 0.085 for the high-sulfur fuel. For the base fuel, there is no statistically significant change in the SMF with distance downstream of the exit plane. For the other fuels, however, there is a significant change, by an order of magnitude, between the 10 and 30 m locations.

E. Comparison of Gas Probe and Particle Probe Data

For a set of runs during the NASA high-aromatic fuel sequences, aerosol emissions were sampled using two gaseous probes: R1-G1 and R1-G4. The gas probe R1-G4 was closest to the 1 m particle probe that was used for all other particulate measurements. It should be noted that the gas sampling train did not provide probe tip dilution. Instead, diluent was added at a point approximately 15 m downstream of the probe tip, where the diluted sample was introduced into a heated sample line. The variation of aerosol parameters with fuel flow rate for these runs is presented in Figs. 11a and 11b. A comparison of these parameters for R1-G4 and the 1 m particle probe are shown in Table 3.

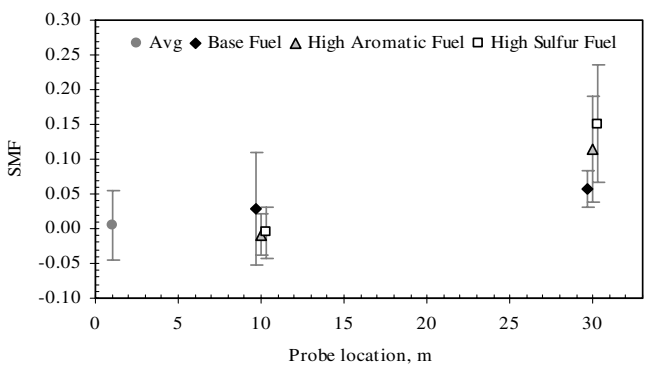

Fig. 10 Soluble mass fraction as a function of probe location.

For the gas vs particle sampling train intercomparison, for a given aerosol, parameters listed in the Table 3, y (y = Dgeom, Sigma, etc.), the percent difference is defined by Eq. (3):

$$\left[\frac{(y_{\text{gas}} - y_{\text{particle}})}{(y_{\text{gas}} + y_{\text{particle}})/2}\right] \cdot 100 \tag{3}$$

Dgeom shows an rms percent difference of 14.9% (scatter) with an average percent difference of −7.2%, where the negative value implies that the gas sampling train mean particle size is systematically 7.2% smaller. This systematic difference is larger than the sum of the uncertainties in the gas and particle mean diameters, as expressed by their rms percent uncertainties shown in the Table 3, hence this systematic difference is statistically significant. Similar relationships hold for the magnitudes of the average differences and uncertainties for Sigma and EI*n*. This indicates that gas-to-particle conversion effects are stronger than loss effects such as agglomeration. In the cases of DgeomM and EI*m*, the average differences are not statistically significant, because for these parameters their systematic differences are smaller than the sum of the uncertainties in their corresponding gas and particle values.

The conditions at this test venue were ideal for minimizing probe effects. The ambient temperature and dew point averaged at 299 ± 5 and $267 \pm 2°$K, respectively, during the entire period of the test. The CFM56-2C1 engine had relatively low-particulate emissions. These factors combined to minimize potential probe effects, such as gas-to-particle conversion, agglomeration, impaction loss, etc. Probe effects could be more significant under less ideal conditions. The results of this analysis show that the use of a gas rather than a particle sampling train influences the resulting data for some parameters to a

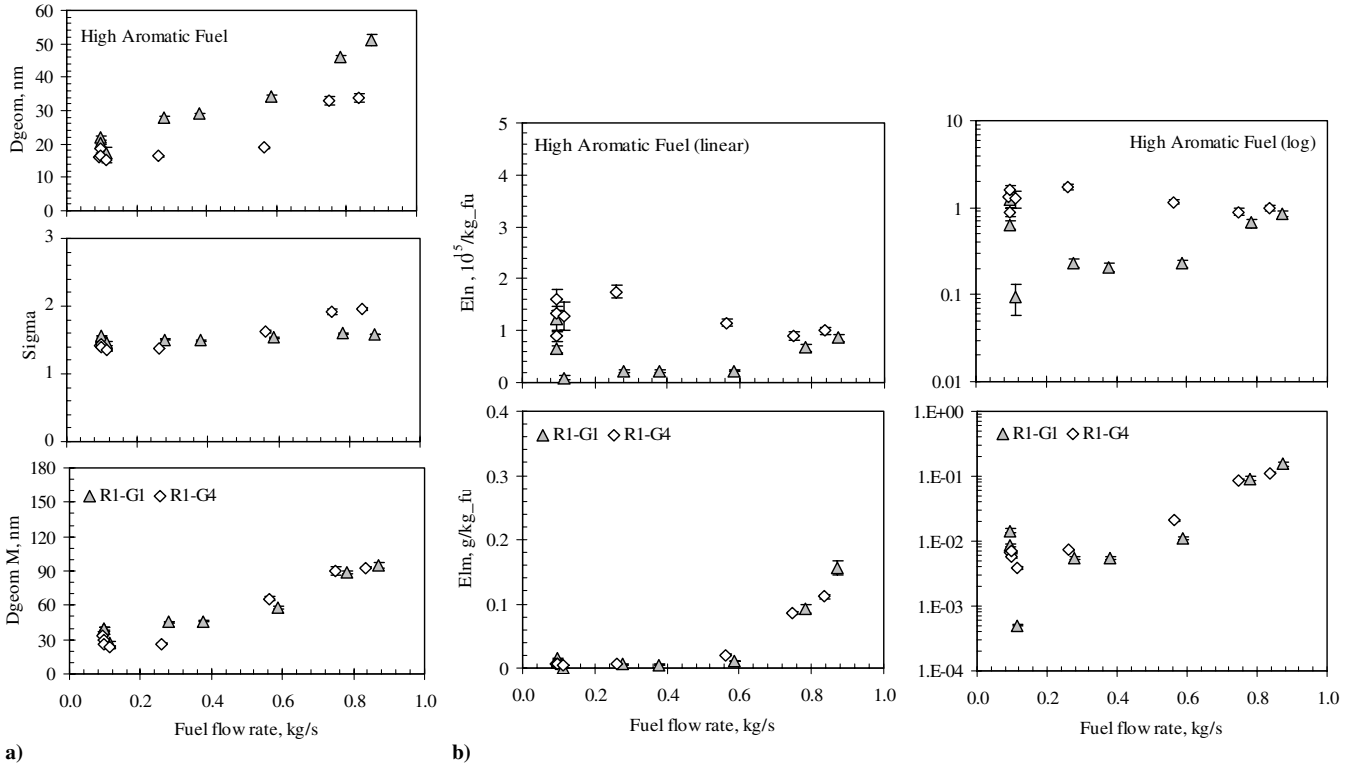

Fig. 11 Variation with fuel flow rate for runs performed with gaseous probes and high-aromatic fuel: a) shape parameters and b) emission indices.

measurable degree even under the ideal conditions encountered in this test. In the gas sampling train, the undiluted gas sample cools as it is transported to the heated section of the sample train where the diluent is also introduced. These conditions are conducive to gas-to-particle conversion in the undiluted section. Gas-to-particle conversion would enhance the small particle concentration thus reducing Dgeom and Sigma and increasing EI*n*, which is observed. Thus gas-to-particle conversion is a serious sample train artifact for gas sampling trains where dilution cannot be achieved at the probe tip.

VI. Conclusions

Data shown here are a summary of the first detailed study of the physical characteristics of the PM emissions from a current in-service commercial class gas turbine engine (CFM56-2C1) as a function of engine operating condition and fuel composition, and as such, provides an introduction to the extensive NASA database from which it is derived. The data summarized here can be applied to emissions estimation, plume evolution model development, and local air quality modeling applications.

The goal of these aerosol measurements was to determine the nature of the emissions at the engine exit plane and the microphysical evolution of the aging plume. Extractive sampling was employed which may result in sample modification due to inertial, thermophoretic, and diffusional processes. In this study, considerable advances have been made in the treatment of these processes, as evidenced by line loss corrections, but further studies are needed, especially to address effects at the probe tip. However, in this study, the uncertainty estimated for line loss, particularly for particles smaller than 20 nm, does not impact the conclusions drawn.

Aerosol properties were calculated for the entire aerosol size distribution and not individual modes. Size distributions for 1 and 10 m were generally lognormal. Strong and sometimes nonlinear dependencies were observed with fuel flow rate. The C/H ratios of the three different fuels used were very similar (∼6.30:1). Based on fuel composition alone, no significant differences in emissions would be expected and no significant differences were observed. This is consistent with previous fuel effect studies [3,50]. The onset of gas-to-particle conversion was apparent at 30 m for low- to medium-fuel flow rates. In this data, nonlognormal size distributions were often observed, where the mean sizes decreased and EI*n* increased relative to the 1 and 10 m size distributions. For high-fuel flow rate data gathered under higher ambient temperature conditions, gas-to-particle conversion was not observed. This result can be explained by shorter plume residence time and warmer ambient air, both of which mitigate against nucleation. Some effect associated with fuel type was observed at 30 m. For the high-sulfur fuel, EI*n* tended to increase; DgeomM and Sigma decreased at low- to moderate-fuel flow rates.

The SMF was found to increase with distance from the engine exit plane. Increasing fuel aromatic and sulfur content are observed to increase the SMF. At both the engine exit plane and at 10 m, the particles contain essentially no soluble material. Evidence of gas-to-particle conversion was observed at 30 m for the aromatic and high-sulfur fuels.

Table 3 Comparison of aerosol parameters for data from the 1 m particle and R1-G4

	Difference between sampling trains		Uncertainties in particle probe measurements		Uncertainties in gas probe measurements	
Parameter	Avg. pct. diff.	RMS pct. diff.	avg. pct. diff.	RMS pct. diff.	avg. pct. diff.	RMS pct. diff.
Dgeom	−7.2	14.9	2.1	2.4	3.2	3.7
Sigma	−4.4	10.2	0.9	1.3	0.9	1.1
DgeomM	−10.0	22.8	5.3	9.6	3.7	5.0
EI*n*	24.7	80.1	7.7	8.9	9.9	11.3
EI*m*	−4.5	59.3	2.4	3.2	3.1	3.5

The intercomparison between gas and particle sampling trains showed that gas-to-particle conversion is a serious sample train artifact for gas sampling trains where dilution cannot be achieved at the probe tip.

Acknowledgments

The authors would like to acknowledge the sponsorship of NASA, and the University of Missouri–Rolla Center of Excellence for Aerospace Particulate Emission Reduction Research throughout the work described in this paper.

References

[1] Schlager, H., Konopka, P., Schulte, P., Ziereis, H., Arnold, F., Hagen, D., Whitefield, P., and Ovarlez, J., "In Situ Observations of Air Traffic Emission Signatures in the North Atlantic Flight Corridor," *Journal of Geophysical Research*, Vol. 102, No. D9, 1997, pp. 10,739–10,750.

[2] Hagen, D. E., and Whitefield, P. D., "Particulate Emissions in the Exhaust Plume from Commercial Jet Aircraft Under Cruise Conditions," *Journal of Geophysical Research, Atmospheres*, Vol. 101, No. 14, Aug. 1996, pp. 19551–19557.

[3] Penner, J. E., Lister, D. H., Griggs, D. J., Dokken, D. J., and McFarland, M. (eds.), *Aviation and the Global Atmosphere*, Intergovernmental Panel on Climate Change Rept., Cambridge Univ. Press, Cambridge, England, U.K., 1999, p. 373.

[4] Haywood, J. M., and Shine, K. P., "Effect of Anthropogenic Sulfate and Soot Aerosol on the Clear-Sky Planetary Radiation Budget," *Geophysical Research Letters*, Vol. 22, No. 5, 1995, pp. 603–606.

[5] Kärcher, B., Peter, T., Biermann, U. M., and Schumann, U., "Initial Composition of Jet Condensation Trails," *Journal of the Atmospheric Sciences*, Vol. 53, No. 21, Nov. 1996, pp. 3066–3083.

[6] DeMott, P. J., Rogers, D. C., and Kridenweis, S. M., "Susceptibility of Ice Formation in Upper Tropospheric Clouds to Insoluble Aerosol Components," *Journal of Geophysical Research*, Vol. 102, No. 16, Aug. 1997, pp. 19,575–19,584.

[7] Heymsfield, A. J., Lawson, R. P., and Sachse, G. W., "Growth of Ice Crystals in Precipitating Contrail," *Geophysical Research Letters*, Vol. 25, No. 9, 1998, pp. 1335–1338.

[8] Detwiler, A., and Pratt, R., "Clear-Air Seeding, Opportunities and Strategies," *Journal of Weather Modification*, Vol. 16, No. 1, April 1984, pp. 46–60.

[9] Grassel, H., "Possible Climatic Effects of Contrails and Additional Water Vapor in Air Traffic and the Environment-Background, Tendencies, and Potential Global Atmospheric Effects," edited by U. Schumann, Springer–Verlag, Heidelberg, Germany, 1990, pp. 124–137.

[10] Sassen, K., "Contrail-Cirrus and Their Potential for Regional Climate Change," *Bulletin of the American Meteorological Society*, Vol. 78, No. 9, Sept. 1997, pp. 1885–1903.

[11] Schumann, U., Strom, J., Busen, R., Baumann, R., Gierens, K., Krautstrunk, M., Schroder, F. P., and Stingl, J., "In Situ Observations of Particles in Jet Aircraft Exhausts and Contrails for Different Sulfur Containing Fuels," *Journal of Geophysical Research*, Vol. 101, No. 3, March 1996, pp. 6853–6869.

[12] Friedl, R. R. (ed.), "Atmospheric Effects of Subsonic Aircraft, Interim Assessment Report of the Advanced Subsonic Technology Program," *NASA Reference Publication 1400*, NASA Goddard Space Flight Center, Greenbelt, MD, 1997, p. 168.

[13] King, M. D., Kaufman, Y. J., Menzel, W. P., and Tanre, D., "Remote Sensing of Cloud, Aerosol and Water Vapor Properties from the Moderate Resolution Imaging Spectrometer (MODIS)," *IEEE Transactions on Geoscience and Remote Sensing*, Vol. 30, No. 1, Jan. 1992, pp. 2–27.

[14] Minnis, P., Garber, D. P., Young, D. F., Arduini, F. F., and Takano, Y., "Parameterizations of Reflectance and Effective Emittance for Satellite Remote Sensing of Cloud Properties," *Journal of the Atmospheric Sciences*, Vol. 55, No. 22, Nov. 1998, pp. 3313–3339.

[15] Fortuin, J. P. F., Van Dorland, R., Wauben, W. M. F., and Kelder, H., "Green House Effects of Aircraft Emissions as Calculated by a Radiative Transfer Model," *Annales Geophysicae*, Vol. 13, No. 4, 1995, pp. 413–418.

[16] Ponater, M., Brinkop, S., Sausen, R., and Schumann, U., "Simulating the Global Atmospheric Response to Aircraft Water Vapor Emissions and Contrails, a First Approach Using a GCM," *Annales Geophysicae*, Vol. 14, No. 9, 1996, pp. 941–960.

[17] Pueschel, R. F., Blake, D. F., Snetsinger, K. G., Hansen, A. D. A., Verma, S., and Kato, K., "Black Carbon (Soot) Aerosol in the Lower Stratosphere and Upper Troposphere," *Geophysical Research Letters*, Vol. 19, No. 16, 1992, pp. 1659–1662.

[18] Solomon, S., Borrmann, S., Garcia, R. R., Portmann, R., Thomason, L., Poole, L. R., Winker, D., and McCormick, M. P., "Heterogeneous Chlorine Chemistry in the Tropopause Region," *Journal of Geophysical Research*, Vol. 102, No. 17, Sept. 1997, pp. 21,411–21,429.

[19] Bekki, S., "On the Possible Role of Aircraft Generated Soot in the Middle Latitude Ozone Depletion," *Journal of Geophysical Research*, Vol. 102, No. 9, May 1997, pp. 10,751–10,758.

[20] Danilin, M. Y., Fahey, D. W., Schumann, U., Prather, M. J., Penner, J. E., Ko, M. K. W., Weisenstein, D. K., Jackman, C. H., Pitari, G., Kohler, I., Sausen, R., Weaver, C. J., Douglass, A. R., Connell, P. S., Kinnison, D. E., Dentener, F. J., Fleming, E. L., Bernsten, T. K., Isaksen, I. S. A., Haywood, J. M., and Karcher, B., "Aviation Fuel Tracer Simulation: Model Intercomparison and Implications," *Geophysical Research Letters*, Vol. 25, No. 21, 1998, pp. 3947–3950.

[21] Samet, J. M., Dominici, F., Curriero, F. C., Coursac, I., and Zeger, A. L., "Fine Particulate Air Pollution and Mortality in 20 U.S. Cities, 1987–1994," *New England Journal of Medicine Medical Progress Series*, Vol. 343, No. 24, 2000, pp. 1742–1749.

[22] Dutton, J. A. (chair), Committee on Aeronautics Research and Technology for Environmental Compatibility Report: for Greener Skies–Reducing Environmental Impacts of Aviation, National Research Council, Washington, D.C., 2002, ISBN: 0-309-08337-0.

[23] Anderson, B. E., Branham, H.-S., Hudgins, C. H., Plant, J. V., Ballenthin, J. O., Miller, T. M., Viggiano, A. A., Blake, D. R., Boudries, H., Canagaratna, M., Maike-Lye, R. C., Onasch, T., Wormhoudt, J., Worsnop, D., Brunke, K. E., Culler, S., Penko, P., Sanders, T., Han, H.-S., Lee, P., Pui, D. Y. H., Thornhill, K. L., and Winstead, E. L., "Experiment to Characterize Aircraft Volatile Aerosol and Trace-Species Emissions (EXCAVATE)," NASA TM-2005-213783, Hampton, VA, Aug. 2005.

[24] Wilson, C. W., Petzold, A., Nyeki, S., Schumann, U., and Zellner, R., "Measurement and Prediction of Emissions of Aerosols and Gaseous Precursors from Gas Turbine Engines (PartEmis): an Overview," *Aerospace Science and Technology*, Vol. 8, No. 2, 2004, pp. 131–143.

[25] Schmid, O., Hagen, D. E., Whitefield, P. D., Trueblood, M. B., Rutter, A. P., and Lilenfeld, H. V., "Methodology for Particle Characterization in the Exhaust Flows of Gas Turbine Engines," *Aerosol Science and Technology*, Vol. 38, No. 11, 2004, pp 1108–1122.

[26] Hagen, D. E., Trueblood, M. B., and White, D. R., "Hydration Properties of Combustion Aerosols," *Aerosol Science and Technology*, Vol. 10, No. 1, 1989, pp. 63–69.

[27] Hagen, D. E., Trueblood, M. B., and Whitefield, P. D., "Field Sampling of Jet Exhaust Aerosols," *Particulate Science and Technology*, Vol. 10, Jan. 1992, pp. 53–63.

[28] Hagen, D. E., Paladino, J., Whitefield, P. D., Trueblood, M. B., and Lilenfeld, H. V., "Airborne and Ground Based Jet Engine Aerosol Emissions Sampling During Two NASA Field Projects: SUCCESS and SNIF," *Journal of Aerosol Science*, Vol. 28, Supplement 1, Sept. 1997, pp. S67–S68.

[29] Hagen, D., Whitefield, P., Paladino, J., Trueblood, M., and Lilenfeld, H., "Particulate Sizing and Emission Indices for a Jet Engine Exhaust Sampled at Cruise," *Geophysical Research Letters*, Vol. 25, No. 10, 1998, pp. 1681–1684.

[30] Hagen, D., Whitefield, P., Paladino, J., Schmid, O., Schlager, H., and Schulte, P., "Atmospheric Aerosol Measurements in the North Atlantic Flight Corridor During Project POLINAT-2," *Journal of Aerosol Science*, Vol. 30, Supplement 1, Sept. 1999, pp. 161–162.

[31] Hagen, D., and Whitefield, P. D., "Study of the Fate of Carbonaceous Aerosol Emissions Through a Gas Turbine Engine," *Air and Waste Management Association Conference Proceedings*, Air and Waste Management Association, Pittsburgh, PA, 2003.

[32] Petzold, A., Busen, R., Baumann, R., Kuhn, M., Strom, J., Hagen, D., Whitefield, P., Baumgardner, D., Arnold, F., Borrmann, S., and Schumann, U., "Near Field Measurements on Contrail Properties From Fuels with Different Sulfur Content," *Journal of Geophysical Research*, Vol. 102, No. 25, 1997, pp. 29,867–29,880.

[33] Whitefield, P., Ross, M., Hagen, D., and Hopkins, A., "Aerosol Characterization in Rocket Plumes," *Journal of Aerosol Science*, Vol. 30, Supplement 1, Sept. 1999, pp. 215–216.

[34] Biskos, G., Reavell, K., and Collings, N., "Description and Theoretical Analysis of a Differential Mobility Spectrometer," *Aerosol Science and Technology*, Vol. 39, No. 6, 2005, pp. 527–541.

[35] Johnson, T., Caldow, R., Pöscher, A., Mirme, A., and Kittelson, D., "New Electrical Mobility Particle Sizer Spectrometer for Engine Exhaust Particle Measurements," Society of Automotive Engineers 2004-01-1341, 2004.

[36] Biskos, G., Reavell, K., Hands, T., and Collings, N., "Fast Measurements of Aerosol Spectra," *Journal of Aerosol Science*, Vol. 34, Supplement 1, 2003, pp. S67–S68.

[37] Hagen, D., Whitefield, P., and Lobo, P., "Performance Evaluation for a Fast Scan Mobility Based Particulate Spectrometer Based on the APEX Data Set," *24th AAAR Conference*, American Association for Aerosol Research, Mt. Laurel, NJ, 2005.

[38] Wey, C. C., Anderson, B. E., Hudgins, C., Wey, C., Li-Jones, X., Winstead, E., Thornhill, L. K., Lobo, P., Hagen, D., Whitefield, P., Yelvington, P. E., Herndon, S. C., Onasch, T. B., Miake-Lye, R. C., Wormhoudt, J., Knighton, W. B., Howard, R., Bryant, D., Corporan, E., Moses, C., Holve, D., and Dodds, W., "Aircraft Particle Emissions Experiment (APEX)," NASA TM-2006-214382, ARL-TR-3903, Cleveland, OH, Sept. 2006.

[39] Montassier, N., Bouland, D., and Renoux, A., "Experimental Study of Thermophoretic Particle Deposition in Laminar Tube Flow," *Journal of Aerosol Science*, Vol. 22, No. 5, 1991, pp. 677–687.

[40] Kittleson, D. B., Abdul-Khalek, I. S., Graskow, B. R., Brear, F., and Wei, Q., "Diesel Exhaust Particle Size: Measurement Issues and Trends," Society of Automotive Engineers TP-980525.

[41] Baron, P. A., and Willeke, K. (eds.), *Aerosol Measurement: Principles, Techniques and Applications*, Wiley, New York, 2001.

[42] Lee, K. W., and Kim, S. P., "Analytical Solutions to Diffusional Deposition of Polydisperse Aerosols in Parallel Plate Channels and Circular Tubes," *Aerosol Science and Technology*, Vol. 31, No. 1, July 1999, pp. 56–65.

[43] Whitefield, P. D., Hagen, D. E., Wormhoudt, J. C., Miake-Lye, R. C., Wilson, C., Brundish, K., Waitz, I., Lukachko, S., Yam, C. K., "NASA/QinetiQ Collaborative Program: Final Report," NASA CR-2002-211900, ARL-CR-0508, Cleveland, OH, Sept. 2002.

[44] Petzold, A., Fiebig, M., Fritzsche, L., Stein, C., Schumann, U., Wilson, C. W., Hurley, C. D., Arnold, F., Katragkou, E., Baltensperger, U., Gysel, M., Nyeki, S., Hitzenberger, R., Giebl, H., Hughes, K. J., Kurtenbach, R., Wiesen, P., Madden, P., Puxbaum, H., Vrchoticky, S., and Wahl, C., "Particle Emissions from Aircraft Engines: a Survey of the European Project PartEmis," *Meteorologische Zeitschrift; Acta Scientiarium Naturalium Universitatis Normalis Hunanensis*, Vol. 14, No. 4, 2005, pp. 465–476.

[45] International Civil Aviation Organization, Aircraft Engine Emissions DataBank, 2006; http://www.caa.co.uk/default.aspx?categoryid=702&pagetype=90.

[46] Wong, H.-W., Miake-Lye, R. C., Zhang, J., Zhang, I. A., and Waitz, I. A., "One-Dimensional Modeling of Particulate Matter Formation from Aircraft Emissions," *APEX 3 Conference* [online database], http://particles.grc.nasa.gov/data/apex3_conf/1129_03_Wong.pdf .

[47] Alofs, D. J., "Performance of a Dual-Range Cloud Nucleus Counter," *Journal of Applied Meteorology*, Vol. 17, No. 9, 1978, pp. 1286–1297.

[48] Alofs, D. J., and Trueblood, M. B., "UMR Dual Mode CCN Counter (Modes: CFD Plus Haze)," *Journal de Recherches Atmosphériques*, Vol. 15, Nos. 3–4, 1981, pp. 219–223.

[49] Li, W., Montassier, N., and Hopke, P., "System to Measure the Hygroscopicity of Aerosol Particles," *Aerosol Science and Technology*, Vol. 17, No. 1, 1992, pp. 25–35.

[50] Paladino, J., Whitefield, P., Hagen, D., Hopkins, A., and Trueblood, M., "Particle Concentration Characterization for Jet Engine Emissions Under Cruise Conditions," *Geophysical Research Letters*, Vol. 25, No. 10, 1998, pp. 1697–1700.

L. Maurice
Associate Editor